frontiers | Frontiers in Marine Science

TYPE Original Research
PUBLISHED 22 August 2022
DOI 10.3389/fmars.2022.1001554

OPEN ACCESS

EDITED BY
Kui Wang,
Zhejiang University, China

REVIEWED BY
Xiaogang Chen,
Westlake University, China Hailong LI,
Southern University of Science and Technology, China

*CORRESPONDENCE
Bochao Xu
xubc@ouc.edu.cn

SPECIALTY SECTION
This article was submitted to Ocean Observation, a section of the journal Frontiers in Marine Science

RECEIVED 23 July 2022
ACCEPTED 08 August 2022
PUBLISHED 22 August 2022

CITATION
Zhao S, Li M, Burnett WC, Cheng K, Li C, Guo J, Yu S, Liu W, Yang T, Dimova NT, Chen G, Yu Z and Xu B (2022) *In-situ* radon-in-water detection for high resolution submarine groundwater discharge assessment.
Front. Mar. Sci. 9:1001554.
doi: 10.3389/fmars.2022.1001554

In-situ radon-in-water detection for high resolution submarine groundwater discharge assessment

Shibin Zhao[1,2,3], Meng Li[4], William C. Burnett[5], Kai Cheng[4], Chunqian Li[4,6], Jinjia Guo[4], Songling Yu[4], Wen Liu[1,2,3], Tong Yang[4], Natasha T. Dimova[7], Guangquan Chen[8], Zhigang Yu[1,2] and Bochao Xu[1,2]*

[1]Frontiers Science Center for Deep Ocean Multispheres and Earth System, and Key Laboratory of Marine Chemistry Theory and Technology, Ministry of Education, Ocean University of China, Qingdao, China, [2]Laboratory for Marine Ecology and Environmental Science, Pilot National Laboratory for Marine Science and Technology (Qingdao), Qingdao, China, [3]College of Chemistry and Chemical Engineering, Ocean University of China, Qingdao, China, [4]College of Information Science and Engineering, Ocean University of China, Qingdao, China, [5]Department of Earth, Ocean and Atmospheric Science, Florida State University, Tallahassee, FL, United States, [6]R & D Center for Marine Instruments and Apparatuses, Pilot National Laboratory for Marine Science and Technology (Qingdao), Qingdao, China, [7]Department of Geological Sciences, University of Alabama, Tuscaloosa, AL, United States, [8]Key Laboratory of Marine Sedimentology and Environmental Geology, First Institute of Oceanography, Ministry of Natural Resources, Qingdao, China

Submarine groundwater discharge (SGD), including both land-based fresh groundwater that enters the ocean from coastal aquifers as well as recirculated seawater that is continuously recharged and discharged on the seabed, has been considered as an important component of the global water and biogenic element (e.g., nitrogen, phosphorus, silicon and carbon) sources and a significant pathway for material exchange at the land-sea interface of coastal ecosystems. Some researchers reported that SGD associated nutrient additions to coastal waters have caused unwanted ecological issues, including red tides, coastal acidification and hypoxia. Natural radon isotope (^{222}Rn, $t_{1/2}$ = 3.8 $_d$) is an excellent tracer for studying SGD and other oceanographic processes including air-sea gas exchange, sediment-water diffusion, and earthquake prediction. However, the conventional radon measurement methods suffer many technical disadvantages. We consequently developed a convenient submersible radon determination approach ("OUC-Rn") using a commercial pulsed ionization chamber (PIC) radon sensor and gas extraction membrane module to produce high precision and high resolution observations. We demonstrate the radon degassing efficiency of the membrane contactor is comparable to the shower-head type air-water exchanger but is independent of operating position. The radon measurement efficiency of the PIC is 2-fold higher than the RAD7 detector and is far less influenced by moisture. We successfully deployed the system in 2.5 meters water depth over a 100 hours period in an anthropogenic influenced bay. Based on our high temporal resolution observations, the SGD flux was estimated to be 0-43.0 cm/d (mean: 25.4 ± 14.5 cm/d). The SGD fluxes pattern plotted

together with the tidal variations revealed that tidal pumping may be the main force driving seawater recirculation into aquifers and thus affecting nutrient, carbon and other dissolved matters dynamics in coastal regions.

KEYWORDS

radon, *in situ* measurement, pulsed ionization chamber, membrane, SGD

1 Introduction

Radon (^{222}Rn, $t_{1/2}$ = 3.8 d) is a powerful tracer for studying geophysical processes including submarine groundwater discharge (SGD) (Burnett and Dulaiova, 2006; Lopez et al., 2020), air-sea gas exchange (Rutgers van der Loeff et al., 2014), sediment-water diffusion (Corbett et al., 1998), and earthquake prediction (Kuo et al., 2010). Recent climate studies combine radon data with biogenic gases (e.g., CH_4 and CO_2) to evaluate the SGD's contribution to atmospheric greenhouse gas budgets (Santos et al., 2019; Chen et al., 2022). Radon-in-water measurements are commonly performed either by discrete grab sampling followed by laboratory analyses (gas extraction, Lucas cells) or by continuous on-site measurements (RAD AQUA-RAD7). While the Lucas cell approach has very high efficiency (close to three hundred percent) (Stinger and Burnett, 2004), a continuous measurement system developed by Durridge, Inc. provides much higher data throughput. In that approach, a radon-in-air analyzer (RAD7) equipped with a Passivated Implanted Planar Silicon (PIPS) alpha detector with energy discrimination is connected to a water-gas exchanger (RAD AQUA) (Burnett and Kim, 2001). After reaching an air-water radon equilibrium, the system can provide continuous on-site radon monitoring of near-surface waters (Burnett and Dulaiova, 2003).

Current limitations of the existing instrumentation for continuous measurements of radon-in-water include: (1) a long response time (>90 min in conventional experimental design, Dimova et al., 2009) to reach both radioactive (^{222}Rn-^{218}Po) and water-air radon equilibrium; (2) relatively low sensitivity; and (3) deployment of key components (power supply, exchanger) above the waterline. Dimova et al. (2009) optimized the water-air equilibrium time of this system by increasing the air and water flow through the exchanger and including an external air pump. However, field experience indicated that with the extra accessories, the system became less versatile and it required additional energy (e.g., generator) to satisfy the higher energy demands of a more powerful water pump. While the energy discrimination is an advantage of this radon detection, a significant disadvantage is the PIPS's sensitivity to humidity in the RAD7's chamber. In addition, the current system is limited to deployment locations that maintain dry conditions for the instrumentation, a significant constraint in some oceanographic applications and under deteriorating weather conditions. Some attempts have been made to measure radon activities *in-situ* using underwater gamma-ray counters based on NaI (Tl) scintillators (Tsabaris et al., 2008; Dulai et al., 2016) or High Purity Germanium (HPGe) detectors (Osvath and Povinec, 2001; Eleftheriou et al., 2020). However, NaI (Tl) applications have high background and low resolution and HPGe systems are costly (Eleftheriou et al., 2013).

Here, we build on the hypothesis that tidal pumping controls the radon temporal variability in coastal water. We present the results of laboratory experiments designed to assess the performance of a novel submersible detection system ("OUC-Rn") compared to the currently available instrumentation. Continuously automated time series measurements were carried for 100 hours from a nearshore fixed platform to delineate high temporal resolution radon behaviors. Our observations imply that SGD may play an important role in driving nutrient biogeochemistry in anthropogenic influenced coastal bay.

2 Materials and methods

2.1 OUC-Rn system setup

The principal components of the OUC-Rn *in-situ* radon detection system include a water-air equilibrator in conjunction with a Pulsed Ionization Chamber (PIC) detector for radon registration (Figure 1).

In working mode, water is continuously pumped through a membrane contactor where radon dissolved in water is degassed and equilibrated with an enclosed air loop in line with the PIC. The selected extraction module (3M Liqui-Cel, Membrana, Germany) for this experimental setup is a commercially available 140-mm long cartridge with an active surface of 0.58 m^2 (MiniModule part number G542). The membrane contactor are polypropylene hollow fiber microporous membranes that are knitted into an array and wrapped around

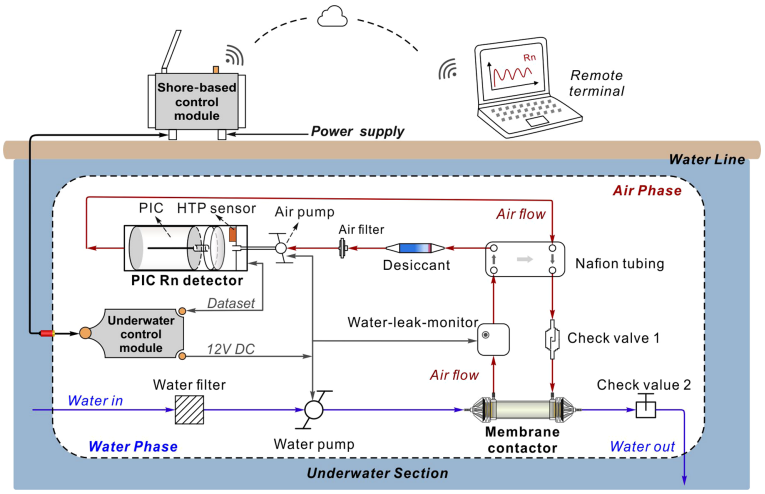

FIGURE 1
Schematic of the *in-situ* OUC-Rn measuring system. The components inside the dash lines are enclosed within a submersible capsule. Filtered water is continuously pumped to a membrane contactor where dissolved radon in water is equilibrated with radon-in-air in a closed air loop. Equilibrated air is directed into the active PIC radon detector after passing through a drying system of a Nafion tubing and desiccant. Two check-valves and a water-leak-monitor prevent any unanticipated reverse flow. A THP sensor monitors the temperature, humidity and pressure within the PIC inner chamber. A shore-based control module provides power to the underwater system and stores real-time data and transmits this information *via* a data cloud to a remote terminal (i.e., cellphone or computer). The figure was hand-drawing utilizing CorelDRAW X8.

a center tube inside a contactor housing (https://www.3M.com/Liqui-Cel). The membrane keeps water and air physically separated, and the unit is not affected by the operational orientation when connected to Rn detector (Schubert et al., 2008). However, turbid waters can clog the membrane relatively quickly; hence contactors generally require relatively clean water with low suspended particulate matter (SPM) concentrations compared to the shower-head Rn extractor which is part of the RAD AQUA system (Wang et al., 2020). To reduce the possibility of suspended particle clogging the extraction module during operation, a pre-filtration device with a 45-μm micro-strainer (Huiante Co., China) is installed at the water inlet of the OUC-Rn system. It is necessary in some situations (e.g., high SPM) to install multistage filtrations.

Radon in the air stream is measured *via* an active self-designed PIC radon detector after being dried by passed through a series of Nafion tubing and desiccant to remove excess humidity. The PIC radon detector is designed with inlet and outlet ports, through which the radon-in-air can circulate in the gaseous phase using a separate air pump (Kamoer Co., China). A commercial PIC sensor (HS Radon Co., China, or FT-lab Co., Korea) and a THP sensor (Bosch Co., Germany) are installed for measuring radon, inner temperature, humidity, and pressure. Detailed descriptions of the PIC sensors can be found elsewhere (Curtiss and Davis, 1943; Seo and Kim, 2021). Briefly, the PIC sensor measures charge pulses created by the ionization of air by α-particles generated from radon decay. It is reported that air with relative humidity up to 80% has only a minor influence on the PIC measuring efficiency since the PIC detects these electrical microspace charges (Seo and Kim, 2021). As a result, the absolute efficiency of a PIC sensor is higher than that of other traditional detectors, such as semiconductor and scintillator detectors affected by moisture (Kada et al., 2010). Despite that, drying units were still implemented in the system to avoid corrosion of the PIC detector (its metal wall and needle) in a high humidity environment. For this set up we used a 144-inch passive Nafion tubing (Durridge, Inc., USA) and a large laboratory drying tube (6.5 cm in diameter and 29.5 cm in height) filled with 8-mesh $CaSO_4$-$CoCl_2$ drierite (W. A. Hammond, Co., USA).

The measured radon-in-air concentration (C_{air}) can be easily converted into radon-in-water concentration (C_{water}) by applying the temperature dependent partitioning coefficient ($K_{w/air}$) via the following Equation 1 (Weigel, 1978; Schubert et al., 2012).

$$C_{water} = C_{air} \cdot K_{w/air} \quad (1)$$

The OUC-Rn system can be powered either by a 12 V battery or by an external AC power supply through an eight-core watertight cable. The maximum power consumption is ~33 W, with both the water and air pumps working. No additional operator intervention is required once the communication between the underwater detection unit and the shore-based control module is established. Data acquisition (as short as one minute) may be programmed at any user's desired integration interval, depending on the expected radon concentration of the samples. For each time step, the user

obtains radon activity, temperature, humidity and pressure automatically stored in a memory device inside the shore-based control module. The dataset transmission, as well as system control, can be controlled by remote terminals with Wi-Fi base (i.e., cellphone and/or laptop). In our experimental unit, we used self-designed software to view the real-time radon activity variation visually from a remote laboratory 20 km away. More details of the OUC-Rn system compared to RAD AQUA-RAD7 are presented in Table 1. Users could also choose to store the real-time data in a memory device inside the underwater capsule, which will make the system completely in-situ.

2.2 High temporal resolution Rn observations and SGD assessment

We conducted an extended time-series radon measurement dock from 27 September 2021 at the Jiaozhou Bay, China (Figure 2A). For this field deployment, the OUC-Rn system was placed at 2.5 meters water depth under a floating platform (Figure 2B). We also deployed a RAD AQUA-RAD7 system on the same platform. The submersible pump for the RAD AQUA-RAD7 set was fixed at the same depth as the OUC-Rn to ensure that both systems sampled the same water. The data collection interval for both systems was set to 30 minutes. A portable CTD-Diver (Schlumberger Co., USA) was attached to the OUC-Rn to monitor changes in temperature and water depths. The time-series measurements were continued for 100 hours, and radon-in-water activities were characterized using a 2-h interval averaging approach to smooth out the statistical scatters. To determine the contribution of ^{222}Rn from ^{226}Ra decay, ^{226}Ra samples were collected by filtering surface water through MnO_2-impregnated acrylic fibers. The fibers were then analyzed for ^{226}Ra *via* a RaDeCC system (Peterson et al., 2009).

A ^{222}Rn mass balance model previously applied to coastal sites was adopted here to calculate the ^{222}Rn flux contributed from SGD input at the Jiaozhou Bay (Lambert and Burnett, 2003; Zhang et al., 2020). In brief, the model accounts for all the ^{222}Rn sources (SGD, ^{222}Rn diffusion from bottom sediments, dissolved ^{226}Ra decay, and input of incoming seawater during flood tides) and sinks (outgoing water during ebb tides, atmospheric evasion, and ^{222}Rn decay) over complete tidal cycles, which is expressed as equation 2.

$$\Delta I/\Delta t = F_{SGD} + F_{sed} + F_{Ra} + F_{in} - F_{out} - F_{atm} - F_{mix} - F_{decay} \quad (2)$$

where $\Delta I / \Delta t$ is the net change of ^{222}Rn inventory between successive measurements (30 min in this study), all ^{222}Rn activities have been corrected for the supported levels by subtracting an average ^{226}Ra activity; F_{SGD} is the ^{222}Rn attributed to SGD; F_{sed} is the ^{222}Rn diffusive flux from bottom sediments; F_{Ra} is the contribution from dissolved ^{226}Ra decay; F_{in} and F_{out} are the ^{222}Rn fluxes induced by tidal input and output, respectively; F_{atm} is the atmospheric evasion flux of ^{222}Rn; F_{mix} is the flux mixing with offshore waters; and F_{decay} is the decay loss of ^{222}Rn.

3 Results

3.1 Efficiency calibration and background of the PIC detector

The efficiency of the PIC detector was determined against a RAD7 (serial #4389) calibrated at Durridge. A natural rock sample (Durridge, Inc., USA) with known radon emanation was prepared as the radon source. The standard rock was sealed for over one month until ^{222}Rn ($t_{1/2}$ = 3.8 d) has reached full secular radioactive equilibrium with its parent ^{226}Ra ($t_{1/2}$ = 1 600

TABLE 1 Comparison of the OUC-Rn versus RAD AQUA-RAD7 radon monitors.

	OUC-Rn	RAD AQUA-RAD7	Notes
Deployment location	underwater (up to 40 m)	Onshore/boat	Entire OUC-Rn, with power supply, could be submerged
Management	remote controlling	site supervision	RAD7 could be remotely controlled by a radio modem
Extraction module	membrane contactor	shower-head exchanger	Membrane contactor is independent of operating position
Components	integrated	decentralized	Water pump and extractor are assembled inside the OUC-Rn
Radon sensor type	PIC [a]	PIPS [b]	PIC lower price but cannot discriminate radon/thoron
Sensitivity [cpm/(Bq/m^3)]	0.0126	0.0066 in Sniff mode [c]	PIC ~90% higher than RAD7, auto/normal modes higher
Operation RH [d]	up to 80%	typical< 10%	High humidity affects the efficiency of RAD7
Background [Bq/m^3]	2.2 ± 1.0	0.2 or less	PIC is 10-fold higher than RAD7
Leakage factor [%/h] [e]	0.068 or 0.36	0.094 or 0.51	RAD7 ~40% higher than PIC
Detection range [Bq/m^3] [f]	3.0 – 10 000	4.0 – 750 000	In the air phase, refer to corresponding manuals
Power requirements	AC or 12 V battery	AC or 12 V battery	Water pumps are the largest power drain
Power supply for sensor	12 V, 0.06 A (0.72 W)	12 V, 1.25 A (15 W)	PIC sensor has less power consumption

[a]Pulsed Ionization Chamber detector; [b]Passivated Implanted Planar Silicon alpha detector; [c]"Sniff" mode only counts $^{218}Po^+$ in RAD7's channel A; [d]Relative humidity of air; [e]Leakages were measured without or with internal air pumps running; [f] RAD7 is more suitable for groundwater and other water samples with high radon-in-water activities.

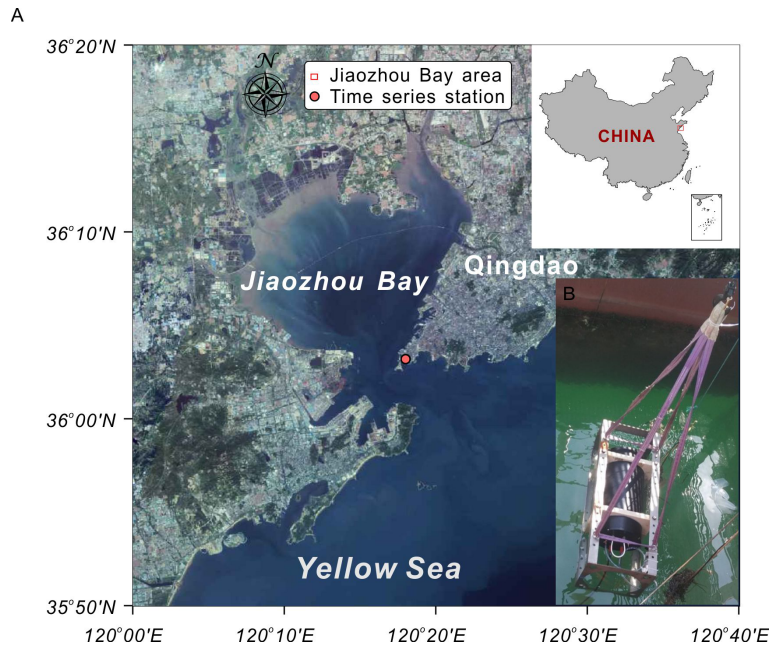

FIGURE 2
(A) Map of the study site in Jiaozhou Bay, China. The area of the Jiaozhou Bay was downloaded from https://www.ovital.com/. **(B)** Long-time series radon measurement was conducted from a fixed platform using the submersible OUC-Rn system.

yr). The RAD7 and PIC detectors were connected in series and a counting protocol was set at 30-min data acquisition with the RAD7 in "Sniff" mode. The radon source/rock standard was connected to the calibration system and the RAD7 internal pump was turned on for five minutes. This allowed uniform distribution of the Rn-enriched air throughout the system of the two detectors. After the rock standard was removed from the system, the air loop was sealed, and we waited for another five minutes to allow any accumulated thoron ^{220}Rn ($t_{1/2}$ = 55.6 s) to decay. Radon data was acquired for at least two hours concurrently by both systems. The radon gas activity (counts per minute, cpm) of the standard sample measured by PIC and RAD7 were averaged at 56 ± 2.4 cpm (n=5) and 29 ± 2.7 cpm (n=5), respectively. These results, expressed in radon sensitivity at 0.0126 cpm/(Bq/m^3) for the PIC detector and 0.0066 cpm/(Bq/m^3) for the RAD7, indicate that the PIC detection efficiency is 1.9 ± 0.19 times higher than the RAD7 used for this study. Further higher efficiency can be accomplished with OUC-Rn system by adding more PIC sensors.

Prior to assessing the intrinsic background of the OUC-Rn, we purged the unit with ultra-pure helium gas and after sealing the unit, set up a counting protocol for 4 hours using 10-min intervals. The background readings of the PIC averaged at 2.2 ± 1.0 Bq/m^3 (n=24) which was about ten times higher than RAD7s (0.2 Bq/m^3 or less, Durridge Com. Inc.). Based on these results, the detection limit of the OUC-Rn system is estimated at 3.0 Bq/m^3 (Currie, 1968).

We also performed a routine gas leakage assessment to ensure radon is not being lost during the operation of the OUC-Rn system. We used the principle that in a closed system with known unsupported radon, the decrease of radon activity could result from either a gas leakage or radioactive decay. For this evaluation, we introduced an air pulse with a relatively high ^{222}Rn into the loop in line with the PIC detector, and then sealed the system by closing the inlet and outlet ports. The ^{222}Rn activities were then monitored for about 24 hours. A parameter "leak factor" was defined as the difference between the observed and theoretical activity based on decay for each time interval (1 h). We determined that the leak factors of the OUC-Rn system are 0.068 %/h and 0.36 %/h without and with the air pump working, respectively (Figures 3A, B). It has been reported that the RAD7 has an average leak rates of 0.094 %/h and 0.51 %/h without and with its inner air pump running (Chanyotha et al., 2014), i.e., about 40% higher than the PIC unit. Since measurements are typically acquired with a 1-h integration time or less, any leakage at these low rates would be well within any expected experimental uncertainties.

3.2 Air-water radon equilibration time

Previous research shows that both water and air flow rates affect the water-gas equilibration time and hence the response to changes in radon concentrations in natural waters

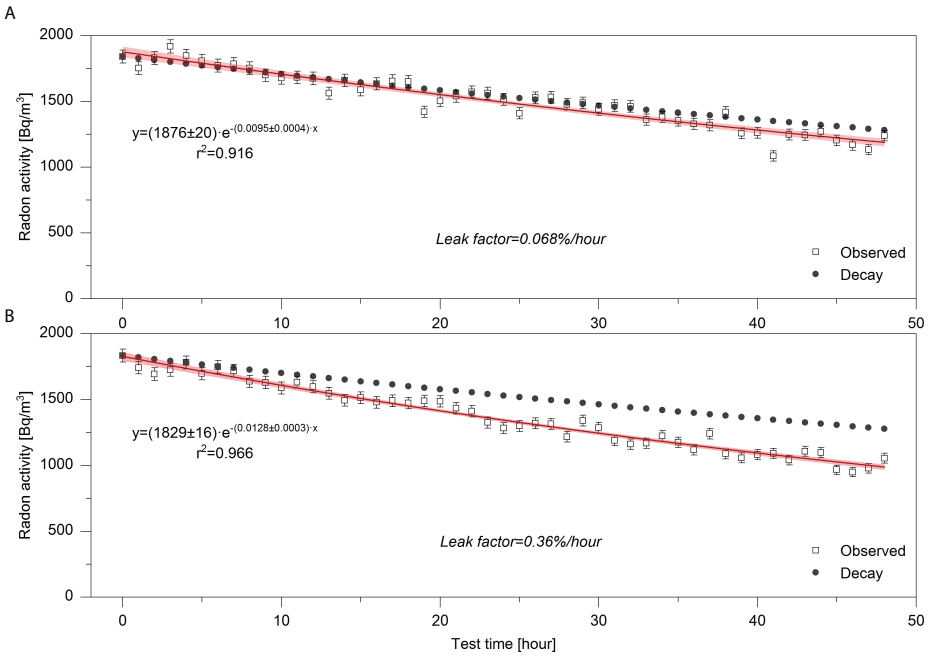

FIGURE 3
The radon activity in a closed air loop observed by PIC sensor (open squares) over time compared to the theoretical ^{222}Rn decay (solid dashes) with the air pump turning off **(A)** or with air pump running **(B)**, respectively. The red shadow areas shown the 95% confident interval based on observed results.

(Dimova et al., 2009). To test the response of the OUC-Rn to abrupt radon in water concentration changes compared to the RAD AQUA, two sets of experiments were designed (Figure 4). The control set consisted of a shower-head exchanger (RAD AQUA) and a RAD7 detector. While the test set consisted of the membrane contactor (3M Liqui-Cel, Membrana, Germany) and another RAD7. We pumped water *via* a tubing that was split so that it delivered the water from the same source to both systems. The two RAD7s were programmed to integrate counts every 10 minutes. Both groups used a drierite desiccant column to remove moisture from the air stream to meet the requirement that the relative humidity in the RAD7 chamber remains below 10%. Measurements were carried out with tap water in the laboratory, which had an essentially steady-state radon activity. In addition, a batch of 50 L distilled water tanks were prepared in advance as a low radon source. Each experiment was first measured in air for 30 minutes to establish a background activity, and then was followed by running tap water for 3 hours, and subsequently the water source was switched to the low radon distilled water until the measured activities stabilized. In this manner, we were able to simulate a low-high-low radon concentration gradient and compare with the response and relaxation times of both the RAD AQUA and membrane contactor under identical conditions. Note that we defined the "response or relaxation time" as the time taken for radon activities to reach 90% of its final concentrations when changing the water pump from low to high concentrations or from high to low.

For the first test, we used a constant air stream flow rate of ~1 L/min *via* the RAD7 internal air pump while varying the water flow rates at 0.5 L/min, 1 L/min, 2 L/min, and 3 L/min, respectively (Figure S1). Based on these tests, the maximum equilibrated activities obtained by these two approaches were similar when the water flow rates ranged from 0.5 L/min to 2 L/min. This result agrees with previous studies (Schmidt et al., 2008). However, the maximum equilibrated activities for the membrane were slightly lower compared to RAD AQUA at a water flow rate of 3 L/min. We attributed this to a shorter contact time between the water and the membrane surface at higher water flow rates. For the equilibrium response/relaxation times of AQUA/membrane contactor, we generally found that at higher water flow rates less time is needed to reach radon concentration equilibrium between the air and water phases when switching between the high and low radon activity scenarios (Figure S1). For example, at 0.5 L/min the equilibrium is reached after about 1 hour, but at a flow rate of 2 L/min equilibration takes only about 30-40 min. This suggests that the membrane contactor has a shorter memory effect than RAD AQUA (Dulaiova et al., 2010).

For the second set of experiments, we kept the water flow rate constant at 1 L/min but varied the airflow rates at 1 L/min, 2 L/min and 3 L/min, respectively (Figure S2). We achieved

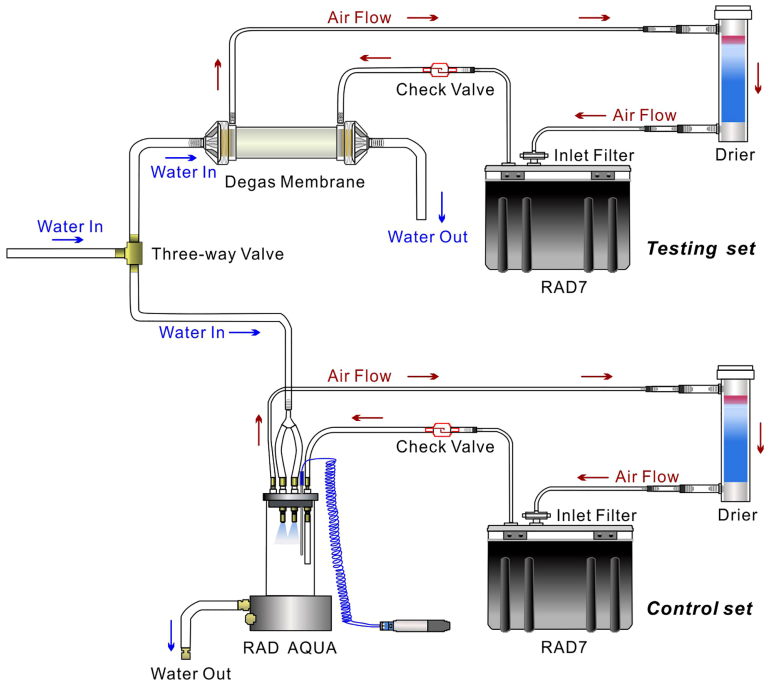

FIGURE 4
Schematic layout of the experimental conditions for examining gas-water equilibration times by two different approaches. The figure was hand-drawing utilizing CorelDRAW X8.

this by adding an external air pump to control the airflow rate while keeping the RAD7 air pumps off. Our results showed that when the airflow rate was increased from 1 L/min to 3 L/min, the degassing efficiency and response/relaxation time of the membrane contactor groups was about the same as that of RAD AQUA groups (Figure S2). Previous work had indicated that increasing the water flow rate (up to 17 L/min) and an airflow rate of 3 L/min can shorten the radon response times in a RAD AQUA-RAD7 system (Dimova et al., 2009). However, we did not attempt to increase the water flow through the membrane contactor to this level as we suspect that the hollow fiber design of the degasser could be damaged. Additionally, adding a powerful air and/or water pump will significantly increase the energy demand and would not be feasible in field conditions. Thus, the optimal experimental conditions for the contractor appear to be using a water flow at 2 L/min and airflow at 1 L/min. We then applied above parameters for the OUC-Rn in the time series field investigations.

3.3 High temporal resolution ^{222}Rn observations

The radon-in-water activities in the coastal area of Jiaozhou Bay ranged from 18.0 ± 2.1 Bq/m^3 to 50.1 ± 3.5 Bq/m^3 (mean: 31.6 ± 6.3 Bq/m^3) as determined by the OUC-Rn system (Figure 5). The test results of the OUC-Rn system are consistent with the RAD AQUA-RAD7 system on the shore within 95% confidence intervals (Figure S3). The long-time series measurements revealed that the variation of radon activities in seawater (~2.5 m water depth) is inversely correlated with the local tides, with radon peaks generally at low tide (Figure 5). The radon activities at 31.0 ± 11.4 Bq/m^3 during a tidal cycle near the same place of the bay were previously documented by Luo et al. (2020), which match well with our results. We measured the ^{226}Ra activities (6.8 ± 0.6 Bq/m^3) of three seawater samples at different tidal times including high and low peaks, indicating that the radon contributed from the ingrowth of ^{226}Ra were limited.

3.4 Radon mass balance model

A conventional ^{222}Rn mass balance model was adopted to calculate the ^{222}Rn flux contributed from SGD input in the Jiaozhou Bay as described below.

3.4.1 Net change of ^{222}Rn inventory between successive measurements

The ^{222}Rn inventory variations in seawater between two successive intervals (i.e., 30 min in our case) was defined as the

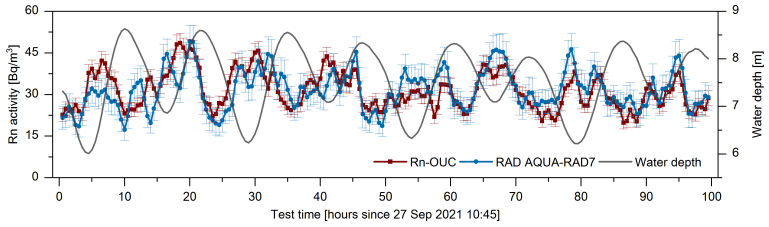

FIGURE 5
A 5-day time-series radon measurement conducted beneath (2.5 m) a fixed floating platform in the Jiaozhou Bay from 27 September to 2 October 2021. The water depths (black line) were measured by a portable CTD-diver using 10-min intervals. The red lines were determined by the OUC-Rn system, while blue lines represent results from the RAD AQUA-RAD7 system. The error bars represent the 2-σ uncertainties based on counting statistics.

excess ^{222}Rn activity (subtracting ^{226}Ra from total ^{222}Rn) multiplying by water depth, which can be calculated with following equation:

$$\Delta I/\Delta t = \frac{I_{t+\Delta t} - I_t}{\Delta t} = \frac{\mathrm{exRn}_{t+\Delta t}\ \Delta\ h_{t+\Delta t}\ -\ \mathrm{exRn}_t\ \Delta\ h_t}{\Delta t} \quad (3)$$

where $I_{t+\Delta t}$ and I_t are the net ^{222}Rn inventory at time $t+\Delta t$ and t , respectively; $h_{t+\Delta t}$ and h_t are the water depth at time $t+\Delta t$ and t , respectively; and $\mathrm{exRn}_{t+\Delta t}$ and exRn_t are the excess ^{222}Rn activities in water column at time $t+\Delta t$ and t .

3.4.2 Diffusive flux from bottom sediments

The diffusion flux depends on diffusion coefficient and concentration gradients of ^{222}Rn in the sediment-water interface, which can be measured with following equation (Martens et al., 1980):

$$F_{sed} = (\lambda_{\mathrm{Rn}} \cdot \varphi \cdot D_m)^{0.5} \cdot (C_{\mathrm{eq}} - C_0) \quad (4)$$

where λ_{Rn} is the decay constant of ^{222}Rn; φ is the porosity of sediment, 0.33 in this study refer to Luo et al. (2020); C_{eq} is the ^{222}Rn activity in pore water that is equilibrium with that in sediment, 4745 Bq/m^3 in this case according to Luo et al. (2020); C_0 is the ^{222}Rn activities in overlying seawater; and D_m is the molecular diffusivity coefficient of ^{222}Rn, as a function of temperature (T) (Peng et al., 1974):

$$D_m = 10^{-\left(\frac{980}{T+273} + 1.59\right)} \quad (5)$$

3.4.3 Tidal effect

In each tidal cycle, ^{222}Rn can be induced to our model box during flooding period and would be removed from the water column with outgoing water on ebb tide. The incoming flux (F_{in}) and outgoing flux (F_{out}) of ^{222}Rn attributed to tidal transportation can be estimated by following equations (Zhang et al., 2016):

$$F_{in} = \frac{h_{t+\Delta t} - h_t}{\Delta t} \cdot [b \cdot {}^{222}Rn_{t+\Delta t} + (1-b) \cdot {}^{222}Rn_{pff} \quad (6)$$

$$F_{out} = \frac{h_{t+\Delta t} - h_t}{\Delta t} \cdot {}^{222}\mathrm{Rn}_{t+\Delta t} \quad (7)$$

where $h_{t+\Delta t}$ and h_t is the water depth at time $t+\Delta t$ and t , respectively; b is the return flow factor (0.92 in this case), based on the tidal prism model refer to Zhang et al. (2020) ; $^{222}\mathrm{Rn}_{t+\Delta t}$ is the ^{222}Rn activity in water column for each time interval; and $^{222}\mathrm{Rn}_{off}$ is the ^{222}Rn activity in offshore water, 15.0 q/m^3 in this case based on the lowest radon activity at the highest tide level.

3.4.4 Atmospheric evasion

^{222}Rn gas will exchange across the surface water and air interface when ^{222}Rn in the two phases is in disequilibrium. The ^{222}Rn fluxes out of the water column by atmospheric evasion can be calculated based on the following equation (MacIntyre et al., 1995).

$$F_{atm} = k \cdot (C_w - \alpha \cdot C_{air}) \quad (8)$$

where C_w is ^{222}Rn activities in seawater; C_{air} is ^{222}Rn activity in atmosphere during continuous measurements (8.4 Bq/m^3 measured by RAD7); α is the radon solubility coefficient that is independent on water temperature (Weigel, 1978); and k is the gas transfer velocity as described by Macintyre et al. (1995).

$$k = 0.45 \cdot \mu^{1.6} \cdot (Sc/600)^{-a} \quad (9)$$

where μ is the wind speed at 10 m elevation; a is a variable power function dependent on wind velocity where $a = 0.6667$ for $\mu \le 3.6$ m/s, and $a = 0.5$ when $\mu > 3.6$ m/s; and Sc is the Schmidt number of ^{222}Rn at a given water temperature and can be calculated based on the formulation as described by Pilson (1998). The wind speed during the entire observation period was in the range of 0.6-7.9 m/s (data from https://www.worldweatheronline.com/).

We have ignored radon decay since it is considered negligible because of the short duration between the time steps in our measurements, i.e. 30 min. The mixing loss (F_{mix}) was estimated based on the maximum negative net ^{222}Rn flux in different periods, which could provide conservative estimations of the SGD flux (Burnett and Dulaiova, 2003). All radon fluxes of sources and sinks in the entire time series investigations were summarized in Figure 6.

4 Discussion

4.1 SGD assessments based on high resolution Rn observations

Based on our high temporal resolution observations, the radon fluxes contributed from SGD were evaluated by applying a radon mass balance model, which varied from 0-143 Bq/m^2/h (mean: 48 ± 31 Bq/m^2/h). Previously reported ^{222}Rn activities in groundwater samples (2 870-7 960 Bq/m^3, mean: 4 560 Bq/m^3) in same season were used as the end-member to calculate SGD fluxes (Luo et al., 2020). Using these values, the SGD fluxes in the Jiaozhou Bay were estimated to be 0-3.1 cm/h (mean: 1.1 ± 0.60 cm/h), i.e., 0-75.1 cm/d (mean: 25.4 ± 14.5 cm/d). The pattern of SGD fluxes plotted together with the tidal variations revealed that the largest peaks generally occur during each transition from the highest high tide to the lowest low tide each 12 hours (Figure 6). We found that the SGD fluxes had a negative correlations with local tidal depth by applying a linear fitting analysis (Figure S4). This indicated the tidal pumping may be the main driving force in this region. Tidal pumping is a common geophysical process driving seawater recirculation into coastal aquifers and thus affecting nutrients and carbon dynamics (Santos et al., 2012).

The SGD fluxes in this bay were previously summarized in a range of 12.3-26.9 cm/d by using the radon mass balance models (Luo et al., 2020). Our results were basically in the scope of former documents. The wide gap of estimated SGD fluxes may be resulting from different sampling seasons, analytical uncertainty of isotopic measurements, varied aquifer types and the activities in groundwater end-members. As described by other investigators, the tracer activity in the groundwater end-member is typically the most sensitive parameter causing the SGD fluxes uncertainty (Cerdà-Domènech et al., 2017; Tan et al., 2018). Note that SGD associated carbon and nutrients additions to the Jiaozhou Bay waters may cause unwanted ecological issues. For example, if we multiply the SGD flux by the average nutrient concentrations of dissolved inorganic N (DIN, 58.4 μmol/L) and P (DIP, 0.61 μmol/L) in coastal groundwater samples (Zhang et al., 2020), the subterranean nutrients discharges were estimated to be (2.7 ± 1.5)×10^7 mol/d for DIN and (2.8 ± 1.6)×10^5 mol/d for DIP, which would be occupied 74% of total DIN input and 82% of

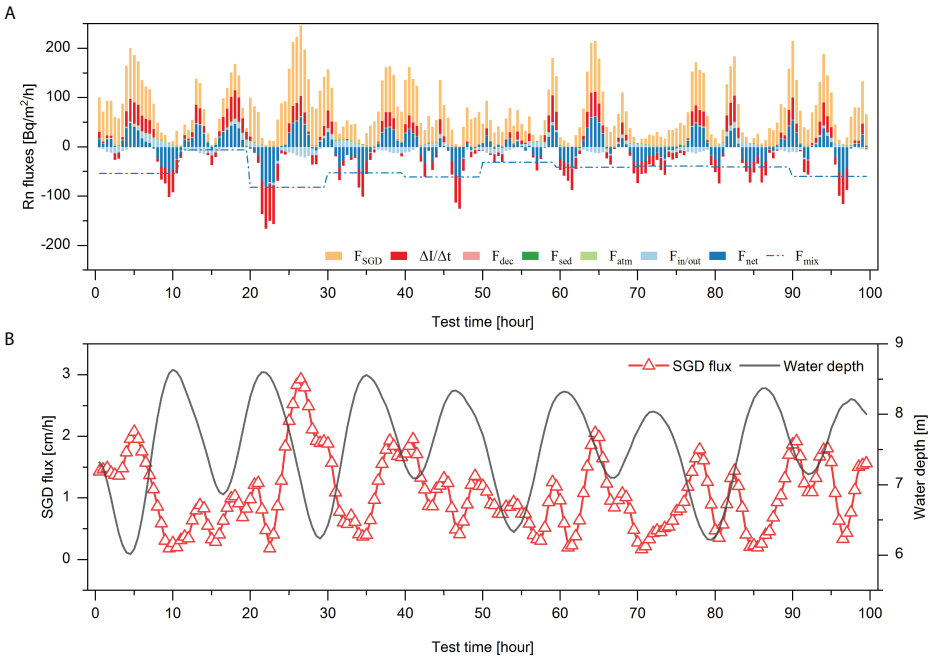

FIGURE 6
(A) Radon fluxes of the sources (SGD, ^{222}Rn diffusion from bottom sediments, dissolved ^{226}Ra decay, and input of incoming seawater during flood tides) and sinks (outgoing water during ebb tides, and atmospheric evasion) in the Jiaozhou Bay during the long-time series measurements. The blue dashed line represents the conservative mixing loss fluxes. **(B)** Temporal variations of SGD flux versus tidal depth during continuous radon investigations.

total DIP input of this regions. Our time series measurements illustrated that SGD may be a potential contributor for the successive occurrences of red tides in this region and maybe other coastal sites worldwide (Wu et al., 2015).

4.2 Perspectives

The submersible OUC-Rn system provides an advanced method to obtain *in-situ* radon activities with high temporal resolution. Since the extraction module is non-selective to the dissolved gases, the PIC sensor could be combined with other gas detection sensors (e.g., CO_2, CH_4, etc.) to allow simultaneous determination of a variety of gases. For example, Li et al. (2021) placed a portable CO_2 sensor on a coastal platform over 35 days and found a trend opposite to the local tides. They speculated that besides the temperature-induced changes in CO_2 solubility, tidal-driven SGD processes were likely an additionally significant contributor to the variation of CO_2 concentrations (Wang et al., 2017). We thus feel that a variety of commercial gas detectors will be useful for acquiring more *in-situ* real-time data to provide insights to better address aquatic scientific concerns (e.g., source-sink of CO_2, and SGD and its associated greenhouse gas emissions).

Taking advantage of lower power consumption, higher detection efficiency and less sensitivity to airborne moisture, the continuous radon monitoring system could be applied to fixed and/or moving observation platforms without supervision. Such platforms could include buoys, subsurface buoys, autonomous underwater vehicles (AUV), autonomous underwater gliders (AUG), remotely operated vehicles (ROVs), etc. Note that the maximum depth for the current system is about 40 meters based on pressure effects on the membrane contactor (~0.4 MPa, 3M Liqui-Cel^{TM}). It would be necessary to build a pressure tight system for deeper measurements to ensure that the pressure decreased to an appropriate range before water entered the extraction module.

Data availability statement

The original contributions presented in the study are included in the article/supplementary material. Further inquiries can be directed to the corresponding author.

Author contributions

SZ conducted data processing and drafted the original manuscript, with later input by BX, WB, ND, and ZY. BX designed the research. ML, KC, and JG performed the system setup and helped with instruments upgrade. SY, WL, TY, and GC was involved sample collection and analysis. All authors edited the manuscript and contributed to general discussion and literature reviews. All authors contributed to the article and approved the submitted version.

Acknowledgments

We thank Guebuem Kim from the Seoul National University for providing valuable suggestions. The authors from Ocean University of China were funded by the Natural Science Foundation of China (41876075, 42130410 and U1906210), and Fundamental Research Funds for the Central Universities, China (201962003).

Conflict of interest

The authors declare that the research was conducted in the absence of any commercial or financial relationships that could be construed as a potential conflict of interest.

Publisher's note

Supplementary material

The Supplementary Material for this article can be found online at: https://www.frontiersin.org/articles/10.3389/fmars.2022.1001554/full#supplementary-material

References

Burnett, W. C., and Dulaiova, H. (2003). Estimating the dynamics of groundwater input into the coastal zone *via* continuous radon-222 measurement. *S. J. Environ. Radioactiv.* 69 (1-2), 21–35. doi: 10.1016/S0265-931X(03)00084-5

Burnett, W. C., and Dulaiova, H. (2006). Radon as a tracer of submarine groundwater discharge into a boat basin in donnalucata, Sicily. *Cont Shelf Res.* 26 (7), 862–873. doi: 10.1016/j.csr.2005.12.003

Burnett, W. C., and Kim, G. (2001). A continuous monitor for assessment of 222Rn in the coastal ocean. *J. Radioanal. Nucl. Ch.* 249 (1), 167–172. doi: 10.1023/A:1013217821419

Cerdà-Domènech, M., Rodellas, V., Folch, A., and Garcia-Orellana, J. (2017). Constraining the temporal variations of Ra isotopes and Rn in the groundwater end-member: Implications for derived SGD estimates. *Sci. Total Environ.* 595, 849–857. doi: 10.1016/j.scitotenv.2017.03.005

Chanyotha, S., Kranrod, C., Burnett, W. C., Lane-Smith, D., and Simko, J. (2014). Prospecting for groundwater discharge in the canals of Bangkok *via* natural radon and thoron. *J. Hydrol.* 519, 1485–1492. doi: 10.1016/j.jhydrol.2014.09.014

Chen, X., Santos, I. R., Hu, D., Zhan, L., Zhang, Y., Zhao, Z., et al. (2022). Pore-water exchange flushes blue carbon from intertidal saltmarsh sediments into the sea. *Limnol. Oceanogr. Lett*. doi: 10.1002/lol2.10236

Corbett, D. R., Burnett, W. C., Cable, P. H., and Clark, S. B. (1998). A multiple approach to the determination of radon fluxes from sediments. *J. Radioanal. Nucl. Ch.* 236 (1-2), 247–252. doi: 10.1007/BF02386351

Currier, L. A. (1968). Limits for quantitative detection and quantitative determination. Application to radiochemistry. *Anal. Chem.* 40(3), 586–593. doi: 10.1021/ac60259a007

Curtiss, L. F., and Davis, F. J. (1943). A counting method for the determination of small amounts of radium and of radon. *J. Res. Natl. Bureau Stand.* 31, 181–190. doi: 10.6028/jres.031.007

Dimova, N., Burnett, W. C., and Lane-Smith, D. (2009). Improved automated analysis of radon (222Rn) and thoron (220Rn) in natural waters. *Environ. Sci. Technol.* 43 (22), 8599–8603. doi: 10.1021/es902045c

Dulai, H., Kamenik, J., Waters, C. A., Kennedy, J., Babinec, J., Jolly, J., et al. (2016). Autonomous long-term gamma-spectrometric monitoring of submarine groundwater discharge trends in Hawaii. *J. Radioanal. Nucl. Ch.* 307 (3), 1865–1870. doi: 10.1007/s10967-015-4580-9

Dulaiova, H., Camilli, R., Henderson, P. B., and Charette, M. A. (2010). Coupled radon, methane and nitrate sensors for large-scale assessment of groundwater discharge and non-point source pollution to coastal waters. *J. Environ. Radioactiv.* 101 (7), 553–563. doi: 10.1016/j.jenvrad.2009.12.004

Eleftheriou, G., Pappa, F. K., Maragos, N., and Tsabaris, C. (2020). Continuous monitoring of multiple submarine springs by means of gamma-ray spectrometry. *J. Environ. Radioactiv.* 216, 106180. doi: 10.1016/j.jenvrad.2020.106180

Eleftheriou, G., Tsabaris, C., Androulakaki, E. G., Patiris, D. L., Kokkoris, M., Kalfas, C. A., et al. (2013). Radioactivity measurements in the aquatic environment using *in-situ* and laboratory gamma-ray spectrometry. *Appl. Radiat. Isotopes* 82, 268–278. doi: 10.1016/j.apradiso.2013.08.007

Kada, W., Dwaikat, N., Datemichi, J., Sato, F., Murata, I., Kato, Y., et al. (2010). A twin-type airflow pulse ionization chamber for continuous alpha-radioactivity monitoring in atmosphere. *Radiat. Meas.* 45 (9), 1044–1048. doi: 10.1016/j.radmeas.2010.07.032

Kuo, T., Lin, C., Chang, G., Fan, K., Cheng, W., and Lewis, C. (2010). Estimation of aseismic crustal-strain using radon precursors of the 2003 m 6.8, 2006 m 6.1, and 2008 m 5.0 earthquakes in eastern Taiwan. *Nat. Hazards.* 53 (2), 219–228. doi: 10.1007/s11069-009-9423-y

Lambert, M. J., and Burnett, W. C. (2003). Submarine groundwater discharge estimates at a Florida coastal site based on continuous radon measurements. *Biogeochemistry* 66 (1/2), 55–73. doi: 10.1023/B:BIOG.0000006057.63478.fa

Li, M., Du, B., Guo, J., Zhang, Z., Lu, Z., and Zheng, R. (2021). A low-cost in-situ CO2 sensor based on a membrane and NDIR for long-term measurement in seawater. *J. Oceanol. Limnol.* 3 (40), 986–998. doi: 10.1007/s00343-021-1133-7

Lopez, C. V., Murgulet, D., and Santos, I. R. (2020). Radioactive and stable isotope measurements reveal saline submarine groundwater discharge in a semiarid estuary. *J. Hydrol.* 590, 125395. doi: 10.1016/j.jhydrol.2020.125395

Luo, M., Zhang, Y., Li, H., Wang, X., and Xiao, K. (2020). Submarine groundwater discharge in a coastal bay: Evidence from radon investigations. *Water-Sui* 12 (9), 2552. doi: 10.3390/w12092552

MacIntyre, S., Wanninkhof, R., and Chanton, J. P. (1995). Trace gas exchange across the air–water interface in freshwater and coastal marine environments. In: P. A. Matson and R. C. Harriss (Eds.), *Biogenic Trace Gases: Measuring Emission from Soil and Water*. United States: Blackwell Science. pp.52–97.

Martens, C. S., Kipphut, G. W, and Klump, J. V. (1980). Sediment-water chemical exchange in the coastal zone traced by in situ radon-222 flux measurements. *Science*. 208(4441), 285–288. doi: 10.1126/science.208.4441.285

Osvath, I., and Povinec, P. P. (2001). Seabed γ-ray spectrometry: Applications at IAEA-MEL. *J. Environ. Radioactiv.* 53 (3), 335–349. doi: 10.1016/S0265-931X(00)00140-5

Peng, T. H., Takahashi, T., and Broecker, W. S. (1974). Surface radon measurements in the North Pacific Ocean station papa. *J. Geophys. Res.: Oceans.* 79 (12), 1772–1780. doi: 10.1029/JC079i012p01772

Peterson, R. N., Burnett, W. C., Dimova, N., and Santos, I. R. (2009). Comparison of measurement methods for radium-226 on manganese-fiber. *Limnol. Oceanogr.: Methods* 7 (2), 196–205. doi: 10.4319/lom.2009.7.196

Pilson, M. (1998). *An Introduction to the Chemistry of the Sea*. Upper Saddle River, New Jersey: Prentice Hall. p. 431.

Rutgers van der Loeff, M. M., Cassar, N., Nicolaus, M., Rabe, B., and Stimac, I. (2014). The influence of sea ice cover on air-sea gas exchange estimated with radon-222 profiles. *J. Geophys. Res.: Oceans.* 119 (5), 2735–2751. doi: 10.1002/2013JC009321

Santos, I. R., Eyre, B. D., and Huettel, M. (2012). The driving forces of porewater and groundwater flow in permeable coastal sediments: A review. *Estuar. Coast. Shelf Sci.* 98, 1–15. doi: 10.1016/j.ecss.2011.10.024

Santos, I. R., Maher, D. T., Larkin, R., Webb, J. R., and Sanders, C. J. (2019). Carbon outwelling and outgassing vs. burial in an estuarine tidal creek surrounded by mangrove and saltmarsh wetlands. *Limnol. Oceanogr.* 64 (3), 996–1013. doi: 10.1002/lno.11090

Schmidt, A., Schlueter, M., Melles, M., and Schubert, M. (2008). Continuous and discrete on-site detection of radon-222 in ground- and surface waters by means of an extraction module. *Appl. Radiat. Isotopes* 66 (12), 1939–1944. doi: 10.1016/j.apradiso.2008.05.005

Schubert, M., Paschke, A., Lieberman, E., and Burnett, W. C. (2012). Air-water partitioning of 222Rn and its dependence on water temperature and salinity. *Environ. Sci. Technol.* 46 (7), 3905–3911. doi: 10.1021/es204680n

Schubert, M., Schmidt, A., Paschke, A., Lopez, A., and Balcázar, M. (2008). *In situ* determination of radon in surface water bodies by means of a hydrophobic membrane tubing. *Radiat. Meas.* 43 (1), 111–120. doi: 10.1016/j.radmeas.2007.12.017

Seo, J., and Kim, G. (2021). Rapid and precise measurements of radon in water using a pulsed ionization chamber. *Limnol. Oceanogr.: Methods* 19 (4), 245–252. doi: 10.1002/lom3.10419

Stinger, E. C., and Burnett, C. W. (2004). Sample bottle design improvements for radon emanation analysis of natural waters. *Health Phys.* 6 (87), 642–646. doi: 10.1097/01.HP.0000137181.53428.04

Tan, E., Wang, G., Moore, W. S., Li, Q., and Dai, M. (2018). Shelf-scale submarine groundwater discharge in the Northern South China Sea and East China Sea and its geochemical impacts. *J. Geophys. Res.: Oceans.* 123 (4), 2997–3013. doi: 10.1029/2017JC013405

Tsabaris, C., Mallios, A., and Papathanassiou, E. (2008). Instrumentation for underwater *in-situ* radon analysis. *Sea Technol.* 49 (3), 21–26.

Wang, X., Li, H., Yang, J., Zheng, C., Zhang, Y., An, A., et al. (2017). Nutrient inputs through submarine groundwater discharge in an embayment: A radon investigation in Daya Bay, China. *J. Hydrol.* 551, 784–792. doi: 10.1016/j.jhydrol.2017.02.036

Wang, Y., Zhang, L., Wang, J., and Guo, Q. (2020). Study on an on-site radon-in-water measurement system based on degassing membrane. *Radiat. Meas.* 131, 106231. doi: 10.1016/j.radmeas.2019.106231

Weigel, F. (1978). Radon. *Chemiker-Zeitung* 9 (102), 287–299.

Wu, B., Lu, C., and Liu, S. (2015). Dynamics of biogenic silica dissolution in jiaozhou bay, western yellow Sea. *Mar. Chem.* 174, 58–66. doi: 10.1016/j.marchem.2015.05.004

Zhang, Y., Li, H., Wang, X., Zheng, C., Wang, C., Xiao, K., et al. (2016). Estimation of submarine groundwater discharge and associated nutrient fluxes in eastern laizhou bay, China using 222Rn. *J. Hydrol.* 533, 103–113. doi: 10.1016/j.jhydrol.2015.11.027

Zhang, Y., Wang, X., Li, H., and Song, D. (2020). Large Inputs of groundwater and associated fluxes of alkalinity and nutrients into Jiaozhou Bay, China. *Hydrogeol. J.* 28 (5), 1721–1734. doi: 10.1007/s10040-020-02144-8